Solutions to Improve Transient Stability of Universal Grid-forming Inverter-based Resources

Author(s): Laaksonen, Hannu

Title: Solutions to Improve Transient Stability of Universal Grid-forming Inverter-based Resources

Year: 2023

Version: Publisher's PDF

Please cite the original version:

Laaksonen, H. (2023). Solutions to Improve Transient Stability of Universal Grid-forming Inverter-based Resources. *International Review of Electrical Engineering (IREE)* 18(3), 164-179. https://doi.org/10.15866/iree.v18i3.23620

This paper is available online at www.praiseworthyprize.org
International Review of Electrical Engineering (I.R.E.E.), Vol. 18, N. 3
ISSN 1827- 6660 May – June 2023

Solutions to Improve Transient Stability of Universal Grid-Forming Inverter-Based Resources

Hannu Laaksonen

Abstract – *In the future power grids, the share of grid-forming inverter-based resources must be increased in order to guarantee stability of the power system during rapid changes in generation, consumption and network topology. Therefore, it is important that the behavior and response of grid-forming inverters is also stable during different types of operation modes, events and faults. Previously, frequency stability improvement of grid-forming battery energy storages with universal frequency-locked-loop after load change in small HV network has been studied. However, in this paper the focus is on more severe disturbances i.e. unbalanced 2-phase and balanced 3-phase faults that are typically most challenging for the different synchronization methods. In this paper, based on multiple PSCAD simulations, new solutions are proposed to improve the transient frequency and voltage stability and fault-ride-through capability of grid-forming inverter-based resources with universal frequency-locked-loop during and after unbalanced and balanced faults.* ***Copyright © 2023 The Authors.***

Keywords*: Distributed Energy Resources, Inverter-Based Resources, Grid-Forming Control, Fault Behavior, Transient Stability*

Nomenclature

BESS	Battery Energy Storage System
DER	Distributed Energy Resources
DSOGI	Dual-Second-Order Generalized Integrator
DSO	Distribution System Operator
FFT	Fast Fourier Transform
FRT	Fault-Ride-Through
GFL	Grid-Following
GM	Grid-Forming
HV	High Voltage
IBR	Inverter-Based Resource
LV	Low Voltage
MC	Momentary Cessation
MSOGI	Multiple-Second-Order Generalized Integrator
MV	Medium Voltage
OLTC	On-Load Tap Changer
PSCAD	Power System Simulation Software
PI-controller	Proportional-Integral controller
PLL	Phase-Locked-Loop
RES	Renewable Energy Resources
SG	Synchronous Generator
TSO	Transmission System Operator
U-FLL	Universal Frequency-Locked-Loop
WT	Wind Turbine
f	Frequency
I_Q	Reactive current
I_0	Zero sequence current
I_1	Positive sequence current
I_2	Negative sequence current
P	Active power
Pf	Active power - frequency
PU	Active power - voltage
Q	Reactive power
QU	Reactive power - voltage
t	Time
U	Voltage
U_1	Positive sequence voltage
U_2	Negative sequence voltage

I. Introduction

I.1. Background

Large-scale integration of Renewable Energy Sources (RES) and Inverter-Based Resources (IBRs) without natural inertia and high fault current feeding capability will change the dynamic behavior of power systems during and after different types of faults. The fault behavior of IBRs needs to be compatible with used protection practices as well as support the transient stability of the power system during major disturbances like faults. This is typically ensured by grid code requirements which specify, for example, IBRs Fault-Ride-Through (FRT) requirements as well as fault current feeding principles during unbalanced and balanced faults. Fault behavior and FRT capability of an IBR is largely determined by its control and

Available online by June 30th, 2023 https://doi.org/10.15866/iree.v18i3.23620

synchronization method and their stability. The main control schemes of IBRs can be divided into Grid-Following (GFL) and Grid-Forming (GFM) methods which can behave differently during disturbances and rapid changes. In the future power systems, the amount of GFM IBRs must be increased to guarantee stability of the power system during rapid changes in generation mix (due to RES) as well as during topology changes and transitions between normal grid-connected and intended islanded (microgrid) operation. Therefore, it is important to ensure that the behavior of GFM IBR is also stable during different types of operation modes, events and faults [1]-[6].

I.2. Fault Behavior Issues of Different IBR Control and Synchronization Methods

This Section provides a brief overview about the fault behavior and transient stability related challenges of GFL and GFM IBRs. Synchronization of GFL and GFM IBRs is one main difference between them and affects also on their fault behavior, fault response and transient stability.

The transient stability refers to the ability to maintain IBR synchronized with the grid during large disturbances like faults. It is of importance because it is also a precondition for the FRT capability of the IBR. During faults, Phase-Locked-Loop (PLL) -based GFLs capability to maintain synchronization is dependent on the voltage drop and to some extent this voltage drop magnitude is also affected by the simultaneous fault current injection of the generating unit. The transient stability of GFLs is dependent on the PLL dynamics as well as on the active or reactive current injection profile during faults. Typically, the grid code also defines the amount of reactive current injection (absolute or relative) during FRT which should be dynamically adjusted based on the connection point voltage magnitude [7]. Different grid synchronization methods [8]-[11] have been proposed for IBRs focusing on immunity against disturbance events (like voltage fluctuations, faults and harmonics) and stability of the synchronization in weak grids [12]. Traditionally, a GFL IBR uses voltage-based grid synchronization [12] i.e. it synchronizes to estimated or measured grid voltage angle e.g. by PLL or Frequency-Locked-Loop (FLL). While most of the GFM IBR control methods don't have a PLL or FLL. Instead, their synchronization could be based, for example, on power synchronization [12], [13] in order to emulate the Synchronous Generators' (SGs') power synchronization principles [14]. Unbalanced, faulty and distorted power system voltages are demanding for all synchronization methods [15]. To get rid of these problems, advancements for PLL- [9], [16] and power-based [13], [17], [18] methods have been proposed [15]. [19] and [20] have proposed Dual-Second-Order Generalized Integrator (DSOGI)-FLL and Multiple-Second-Order Generalized Integrator (MSOGI)-FLL, respectively, as a suitable solutions to detect fundamental-frequency negative and positive-sequence components of the phase voltages. In order to protect the semiconductors of GFM IBRs during balanced fault, the IBR control should limit the magnitude of the fault current, feed fault current and support fault recovery [21]. Fault current can be limited in different ways e.g. by current, virtual impedance or voltage limiters [21]. Based on [21], emerging challenges of the GFM IBRs include transient overvoltage, temporary overcurrent, undesired current saturation and unspecified output current vector angle. In contrast to the SGs, IBRs' limited overcurrent capability needs also use of current magnitude limiting control methods and this creates additional limitation to the transient stability of GFM IBRs [12], [22]. According to [21], the open issues of the current-limiting GFM IBRs include, for instance, transient stability evaluation and voltage source operation during overcurrent situations as well as voltage controllers' windup. Reactive power (Q) droop control loop as well as full reactive current (I_Q) injection [23], required often from larger Distributed Energy Resource (DER) units by grid code requirements, can weaken the transient stability of GFM IBRs [12], [24]. During unbalanced grid faults, some grid codes also require dual-sequence current injection [25]. Typically, IBRs have been designed to reduce the negative sequence current (I_2) contribution partially or entirely during unbalanced faults and this can lead to maloperation of protection functions which are based on I_2 contribution detection [1], [26]. Therefore, alternative protection solutions are required or I_2 contribution should be requested from the DER by the grid codes (like in Germany [1]). If the I_2 contribution is requested from the DER unit during unbalanced faults (e.g. 2-phase short-circuit faults), according to [26], the fed current may also decrease the negative sequence voltage (U_2) and decrease the voltage phase unsymmetry. On the other hand, I_2 injection simultaneously limits the control capability of the DER current in the positive sequence (I_1) [26]. From the protection viewpoint, GFMs' short-circuit response and ability to feed negative- (I_2) (and zero, I_0) sequence fault current during unbalanced faults needs to be known [27]. In [28], it was stated that GFMs have more challenges from faults in strong grids and GFLs have more challenges from faults in weak grids. [14] notified also that the GFM IBRs can have challenges related to, angle stability, FRT capability, and transition from islanded to grid-connected mode. In addition, unintentional islanding of GFM IBRs can be a challenge, because GFMs use different variables for islanding detection than GFLs [29]. Table I tries to briefly summarize the fault behavior and transient stability challenges as well as the open issues of GFL and GFM IBRs based on the literature. [30] analyzed also active and reactive fault current support from IBR-based generation and their impact on the recovery speed of the system voltage. It was concluded that impact of active fault current is very obvious when the dynamic load component ratio is more than 20%. It was proposed in [30] that the fault behavior of the IBRs should take into account the types of loads in the same network area.

TABLE I
SUMMARY ABOUT FAULT BEHAVIOR AND TRANSIENT STABILITY RELATED CHALLENGES AND OPEN ISSUES OF GFL AND GFM IBRS

	GFL inverter	GFM inverter
Challenges and Open Issues	• During faults PLL can lose track of grid frequency; • GFLs suffer larger impacts from faults in weak grids; • Negative sequence current suppression during unbalanced faults may lead to protection maloperation; • Momentary cessation mode	• Desynchronization during faults, e.g. full reactive current injection during fault may cause desynchronization; • Can need adaptation of load shedding and protection settings; • Reactive power droop control loop can negatively affect the transient stability of GFMs; • Negative sequence current suppression during unbalanced faults may lead to protection maloperation; • Control related to current limiting limits also transient stability of GFMs; • Transient overvoltage, temporary overcurrent, undesired current saturation and unspecified output current vector angle; • GFMs suffer greater impacts from faults in strong grids; • Momentary cessation mode; • Transition to grid-connected mode from islanded mode can be challenging; • GFM inverters' islanding unintentionally can be a risk; • Current-limiting GFM IBRs' unresolved matters: transient stability evaluation and operation as voltage source during overcurrent situations as well as voltage controllers' windup.

In [31], for example, also some potential solutions have been proposed to overcome fault behavior challenges of GFM IBRs related to transient angle instability and limitation of short-circuit currents. Also, for instance, in [32] two control methods to enhance transient stability during faults were proposed i.e. for overcurrent protection a virtual impedance control method and for IBRs grid connection support an adaptive inertia control scheme.

[33] highlighted that apart from the GFM control method, the frequency reference is in key role in the system performance.

In a quite recent grid code [21], [34] GFM IBRs are required to start the reactive current (I_Q) feeding to the power system in less than 5 ms when the connection point voltage (U) is under 0.9 pu.

In the recently proposed Great Britain (GB) grid code for GFM IBRs [35], it has been also stated, for instance, that fast fault current injection of GFM IBR must fulfill the requirements related to short-circuit current contribution capability ($\geq$ 1.5 pu) and response time depending on the type of fault and depth of voltage dip due to the fault as well as GFM IBR damping factor should be between specified limits etc.

On the other hand, in some grid codes, one challenge has been so called Momentary Cessation (MC) mode of IBRs [36]. In MC mode, IBRs temporarily cease both active (P) and reactive power (Q) feeding to the grid when the voltage U drops or rises severely. Due to the increase of IBRs in power systems, the MC function can negatively affect the transient stability of the traditional generators when MC operation reduces power fed from IBRs to the loads [36].

I.3. Objectives and Organization

In the future renewable-based variable inertia power systems with high amount of GFM IBRs, it is important that their stability during faults can be ensured. In addition, their fault behavior and response needs to be compatible with the existing or new distribution and transmission network protection schemes during grid-connected and islanded operation.

In this paper, recently proposed new grid-forming and grid-supporting Universal Frequency-Locked-Loop (U-FLL) -based synchronization method [37] is utilized with IBRs in multiple PSCAD simulations. In general, target of the recent U-FLL method is that it would be suitable for different types of future power systems with different share of rotating SGs and GFM/GFL IBRs (including also island operated microgrids).

In [37], the general functionality, applicability and feasibility of the new U-FLL method, its frequency stability improvement when compared e.g. to traditional PLL-based DERs / IBRs and fulfillment of the set U-FLL's general targets 1) - 4) (Section II) have already been presented.

After that, in [38] the frequency stability effect of U-FLL-based battery energy storages location, enhanced control schemes and operation mode was studied with a focus on frequency stability after load change in small HV network. However, in this paper the focus is on more severe disturbances i.e. unbalanced 2-phase and balanced 3-phase faults which are typically most challenging for the different synchronization methods of IBRs. The target of this paper is to study different solutions to improve the transient stability, fault behavior and FRT capability of U-FLL-based IBRs with a focus on the effect of different U-FLL modifications. In the simulations of this paper, 2- and 3-phase short-circuit faults are studied mainly during islanded operation with a focus on:

- The effect of DER unit's synchronization method and additional negative sequence current (I_2) injection during unbalanced 2-phase faults (during MV islanded operation) on transient stability;
- The effect of U-FLL inputs and communication delay on transient stability of the DER unit during balanced 3-phase faults;
- The effect of the operation mode of Battery Energy Storage Systems (BESSs) on transient stability (simple HV network model);
- The effect of U-FLL modifications on transient stability during 3-phase faults (HV network model).

Next in Section II the grid-forming/-supporting U-FLL synchronization for IBRs is briefly presented. After that, Section III shows the simulation models and study cases with variable shares of IBRs and SGs. Then, the results from the simulations are presented in Section IV and finally in Section V the conclusions are stated.

II. Universal Grid-Forming Synchronization Method for IBRs

At the moment, no universal GFM synchronization and control scheme exists. For this reason, U-FLL-based synchronization for IBRs has been recently proposed in [37]. Figs. 1 present the U-FLL and its PSCAD implementation. General targets 1) - 6) for the new U-FLL have been presented in [37]. Regarding to these targets and especially islanding detection, in [39] it was concluded that the U-FLL GFM method does not risk the operation of the traditional passive islanding detection schemes unlike some other commonly proposed GFM control methods. More information about details of U-FLL can be found from [37].

III. Study Cases and Simulation Models

The key study cases of this paper are summarized in Table II and used DER and network models are presented in Figs. 2-9.

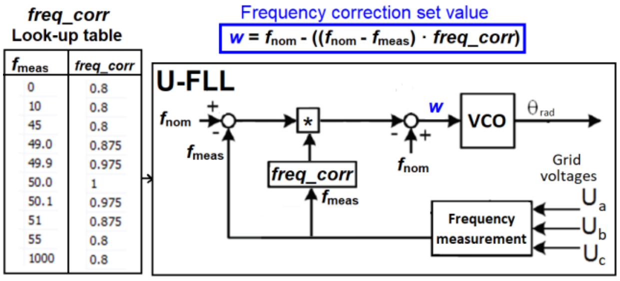

(a)

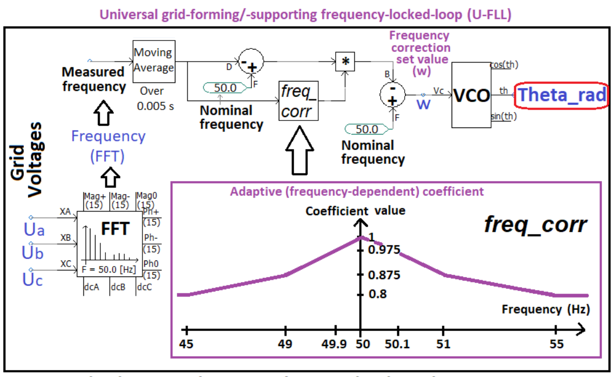

Synchronization angle (Theta_rad) determination with U-FLL component during grid-connected/islanded operation

(b)

Figs. 1. (a) Proposed universal grid-forming and supporting U-FLL synchronization method and (b) PSCAD implementation of U-FLL

TABLE II
KEY STUDY CASES (Figs. 2-9)

Case	Voltage level	Types and number of generating units	Synchronization of IBRs
CASE_1_MV_HYBRID	MV	WT (1, full power conv.), SG (1)	U-FLL
CASE_2_HV_HYBRID	HV	BESS (16), SG (1)	PLL or U-FLL
CASE_1_MV_IBR / CASE_1_LV_IBR	MV and LV	WT (1, full power converter), BESS (1)	U-FLL
CASE_2_HV_IBR	HV	BESS (68)	U-FLL

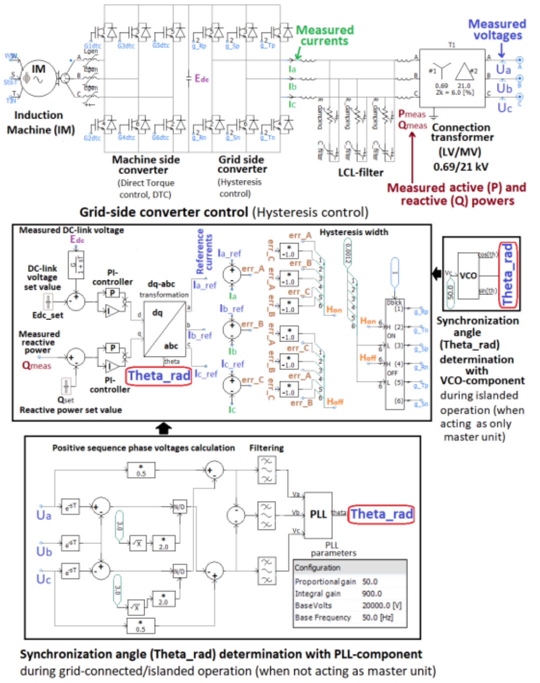

Fig. 2. Detailed PSCAD model of wind turbine, WT, with full power converter control scheme without utilization of new U-FLL (Figs. 1) in CASE_1_MV_HYBRID (Fig. 5) and CASE_1_MV_IBR (Fig. 8) [37]

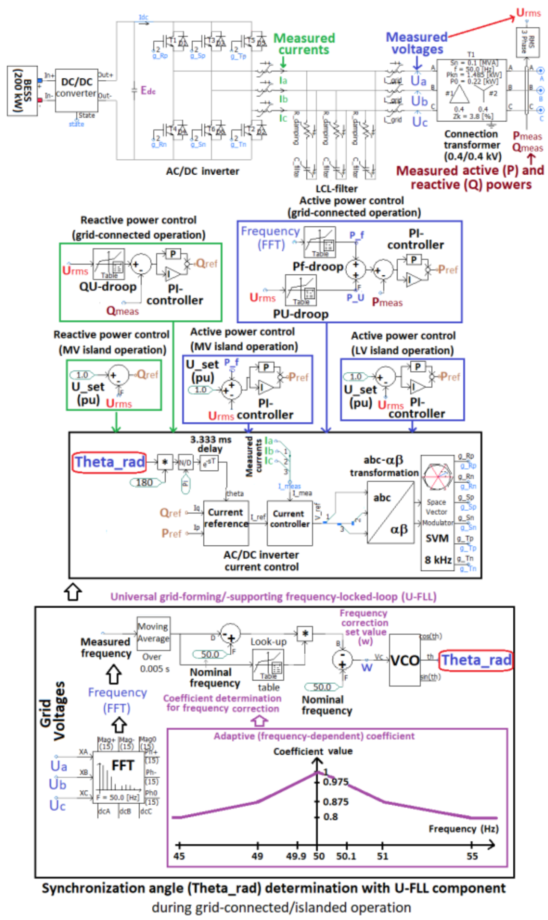

Fig. 3. Detailed PSCAD model of battery energy storage system, BESS with AC/DC-inverter control scheme including new U-FLL (Figs. 1) [37]

For example, following issues were studied and compared in the study cases (Table II and Section IV):

- 100 % IBR (MV & LV), *CASE_1_MV_IBR* and *CASE_1_LV_IBR* (Fig. 8):
  - The effect of DER unit's U-FLL input and additional negative sequence current (I_2) injection during unbalanced 2-phase faults (during grid-connected and MV islanded operation) on transient stability;
  - The effect of U-FLL input on transient stability of the DER unit during balanced 3-phase faults.
- Hybrid (MV), *CASE_1_MV_HYBRID*, (Fig. 5):
  - The effect of U-FLL input and communication time delay on transient stability of the DER unit during balanced 3-phase faults.
- Hybrid (HV), *CASE_2A_HV_HYBRID* and *CASE_2B_HV_HYBRID* (Fig. 7):
  - 2- and 3-phase short-circuit faults (200 ms and 100 ms) in the middle of the HV line at t=15.0 s;
  - Effect of DER control/synchronization method & BESSs operation mode.
- 100 % IBR (HV), *CASE_2_HV_IBR* (Fig. 9):
  - Effect of different U-FLL modifications during 3-phase faults.

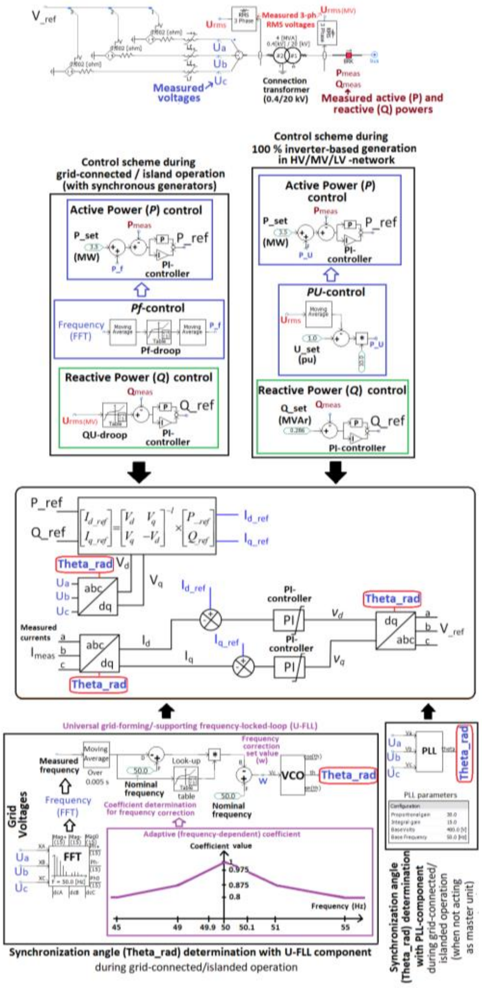

Fig. 4. BESS's average PSCAD model with controlled voltage sources and control scheme with new U-FLL (Figs. 1) or traditional PLL [37]

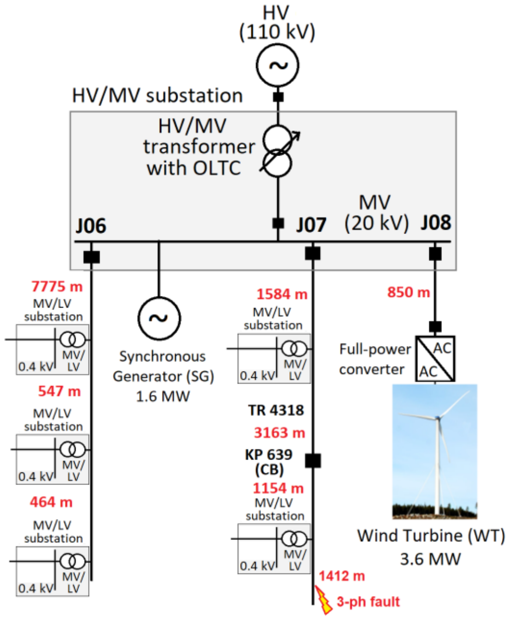

Fig. 5. One-line diagram of the MV hybrid network with IBR (Fig. 2) and SG (CASE_1_MV_HYBRID)

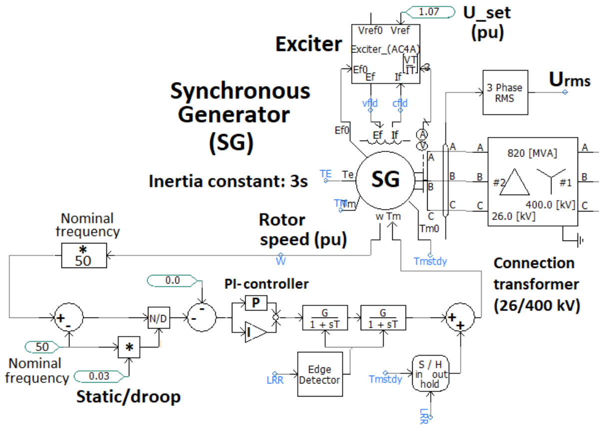

Fig. 6. SG's (HV network connected) PSCAD model used in CASE_2A_HV_HYBRID and CASE_2B_HV_HYBRID (Fig. 7) [37]

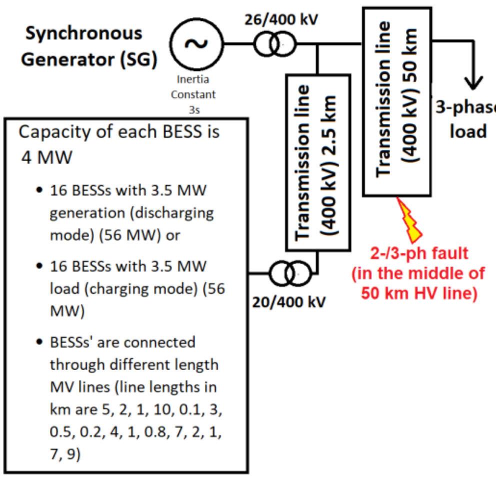

Fig. 7. One-line diagram of the hybrid small HV network with 16 BESSs (Fig. 4) and SG (Fig. 6) (CASE_2A_HV_HYBRID) and (CASE_2B_HV_HYBRID)

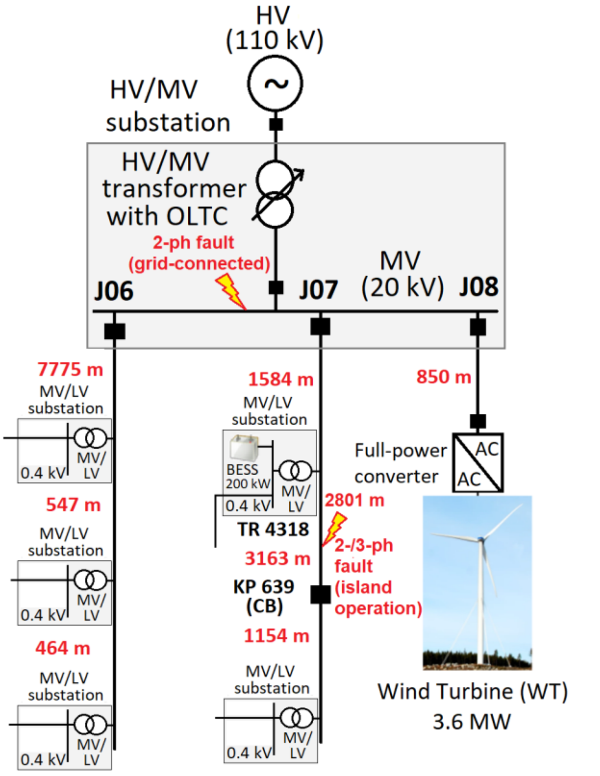

Fig. 8. One-line diagram of the 100 % IBR-based MV and LV network with WT (MV network, Fig. 2) and BESS (LV network, Fig. 3) in CASE_1_MV_IBR and CASE_1_LV_IBR

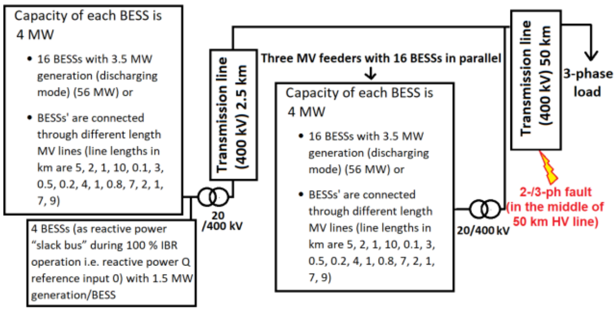

Fig. 9. One-line diagram of the 100 % IBR-based small HV network with 68 BESSs (in MV network, Fig. 4) in CASE_2_HV_IBR

IV. Simulation Results

In this Section IV, the key simulation results from the various study cases (see Section III and Table II) are shown. First, in Section IV.1 simulation results with 100 % IBR-based generation in MV and LV microgrids (CASE_1_MV_IBR and CASE_1_LV_IBR, Fig. 8 and Table II) are shown. Then, Section IV.2 presents the results from cases with hybrid MV microgrid (CASE_1_MV_HYBRID, Fig. 5 and Table II). After that, Section IV.3 shows the results from hybrid small HV network cases (CASE_2A_HV_HYBRID & CASE_2B_HV_HYBRID, Fig. 7 and Table II). Finally, Section IV.4 presents the results from case with 100 % IBR-based generation in small HV network (CASE_2_HV_IBR, Fig. 9 and Table II).

IV.1. 100 % IBR MV and LV Microgrid

The total simulation time in Section IV.1 subcases was t=4.0 s, transition to MV islanded (microgrid) operation with WT (Fig. 2) and BESS (Figs. 3 and 8) happened at t=1.9 s and transition to LV islanded operation with BESS (Fig. 3) happened at t=2.7 s. In all simulations unbalanced 2-phase or balanced 3-phase short-circuit happened between t=2.4-2.55 s. In addition, in simulations with 2-phase short-circuit happened during grid-connected operation at t=0.75-0.9 s.

IV.1.1. Effect of Negative Sequence Current Injection During Unbalanced Fault

Next the results with 100 % IBR-based generation in CASE_1_MV_IBR and CASE_1_LV_IBR (Fig. 8 and Table II) subcases (Table III) during unbalanced 2-phase short-circuit are shown in Figs. 13 and 14. The control scheme differences of WT and BESS in the studied subcases are presented in Table III and Figs. 10-12.

Unlike SGs, IBRs do not necessarily inject I_2-current during unbalanced faults.

Therefore, additional I_2-current feeding may be required (e.g. by grid codes) in order to avoid maloperation of some traditional protection functions used in transmission or distribution networks. The purpose of the simulation studies (Table III) in this Section was to examine the effect of the DER unit's U-FLL input modification (on both WT and BESS) and I_2-current injection (on WT) during unbalanced 2-phase faults (during grid-connected and MV islanded operation) on transient frequency and voltage stability. In addition, the aim was to compare the fault behavior of WT between the grid-connected and islanded operation modes. From the simulation results (Figs. 13-15), it can be seen that in the grid-connected operation the U-FLL input differences and additional I_2 injection do not affect much on the frequency and voltage stability (Figs. 13).

TABLE III
CONTROL SCHEME DIFFERENCES IN SUBCASES OF CASE_1_MV/LV_IBR (FIGS. 8 AND 10-12, TABLE II) DURING UNBALANCED 2-PHASE FAULTS

Subcase $^{*)}$	WT control (MV network)	WT $^{**)}$ and BESS $^{***)}$ U-FLL
CASE_1_MV/LV_IBR_1A (U-FLL)	Without additional I_2-feeding	Input frequency measurement with 15 harmonics from FFT (Base case), Figs. 2-3
CASE_1_MV/LV_IBR_2A (U-FLL)	With additional I_2-feeding, Fig. 11	Input frequency measurement with 15 harmonics from FFT (Base case), Figs. 2-3
CASE_1_MV/LV_IBR_2B (U-FLL)	With additional I_2-feeding, Fig. 11	With upper and lower limits for frequency correction set value (w), Fig. 10
CASE_1_MV/LV_IBR_2C (U-FLL)	With additional I_2-feeding, Fig. 11	Frequency calculated from MV side filtered positive sequence voltages, Fig. 12

$^{*)}$All subcases with U-FLL , $^{**)}$ LV side phase voltages are utilized for frequency measurement with FFT if not otherwise stated, $^{***)}$ Control with I_2-filtering

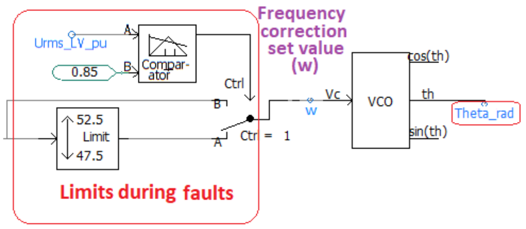

Fig. 10. With upper and lower limits for frequency correction set value (w) in U-FLL of WT and BESS during faults (Table III)

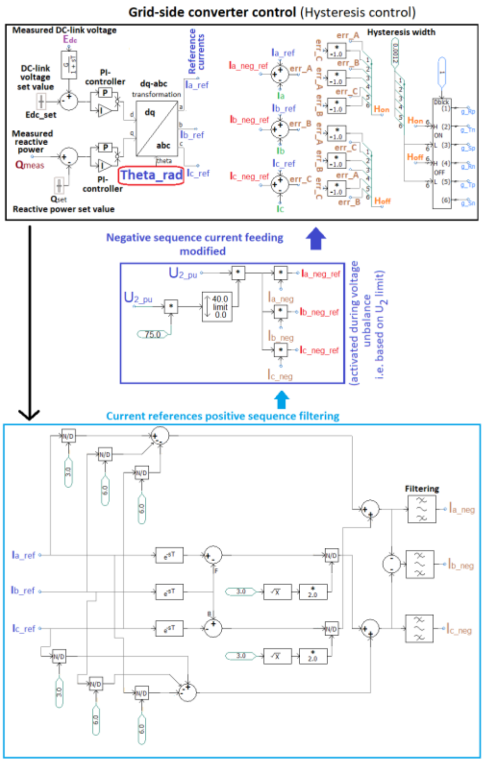

Fig. 11. With upper and lower limits for frequency correction set value (w) in U-FLL of WT and BESS during faults (Table III)

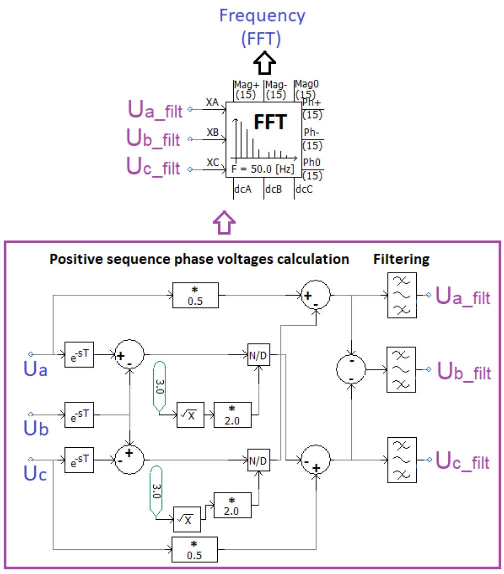

Fig. 12. With frequency calculated from positive sequence voltages for input U-FLL in WT and BESS control scheme during faults (Table III)

However, it can be noted that the additional I_2-current feeding by the WT (Fig. 14(b)) seems to reduce WT's active power (Fig. 15(a)) during 2-phase fault in grid-connected operation. Simultaneously, the reactive power output of the WT (Fig. 15(b)) remained quite similar in the different cases. In addition, based on Figs. 13(b) and 14(b) I_2-current feeding of the WT did not support/affect positive sequence voltage (U_1) or reduce the negative sequence voltage (U_2) at the WT connection point during grid-connected operation. However, it should be noted that the 2-phase fault happened at the MV bus during grid-connected operation (Fig. 8). Effect could have been different if the 2-phase fault would have happened further away from the HV/MV substation (Fig. 8). On the other hand, based on the simulation results (Figs. 13-15) WT control with additional I_2-current feeding will worsen the frequency (Fig. 13(a)) and voltage (Fig. 13(b)) stability during and after 2-phase fault in islanded operation mode. In addition, it can be seen that the input of U-FLL also has an impact on frequency and voltage stability (Figs. 13). In this regard, it can be seen (Figs. 13-15) that when the additional I_2-current feeding of the WT is active, it is beneficial to utilize frequency calculated from the positive sequence voltages (Fig. 12) as an input for U-FLL of WT (and BESS) (CASE_1_MV/LV_IBR_2C (U-FLL)).

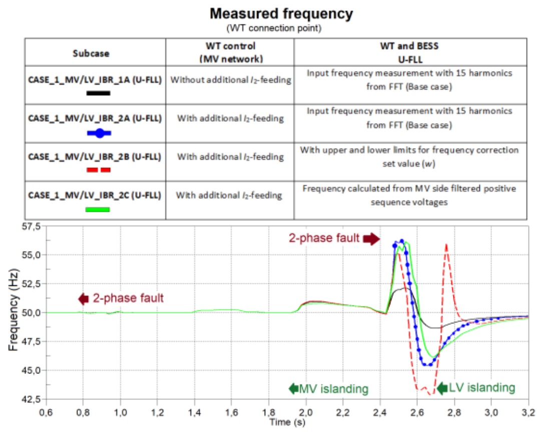

(a)

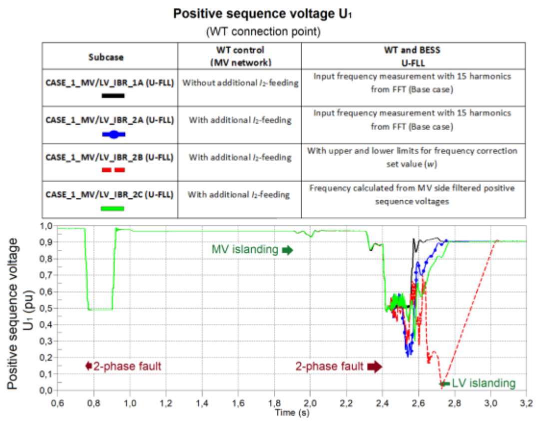

(b)

Figs. 13. (a) Measured frequency and (b) positive sequence voltage (U_1 in per unit, pu) at the WT connection point (Figs. 8, 10-12 and Tables II, III)

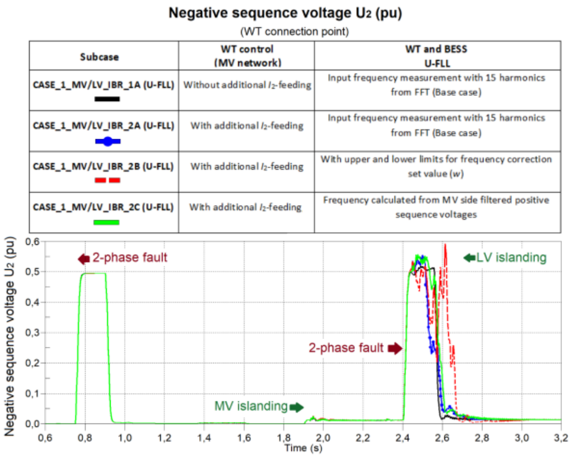

(a)

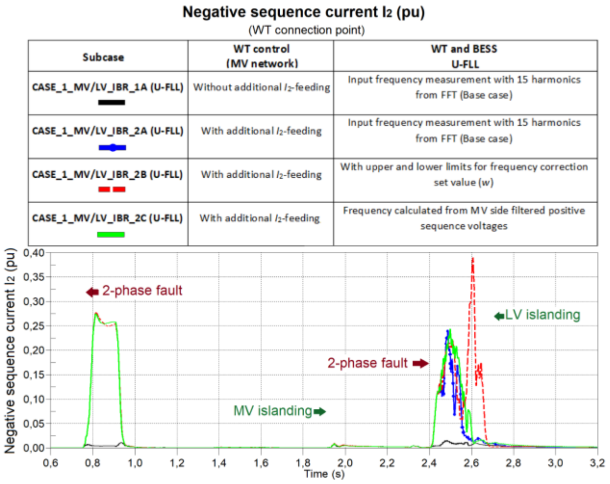

(b)

Figs. 14. Negative sequence (a) voltage U_2 and (b) current I_2 at the WT connection point (Figs. 8, 10-12 and Tables II, III)

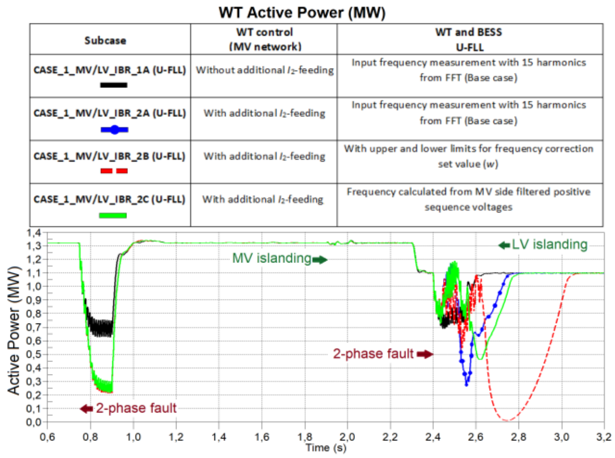

(a)

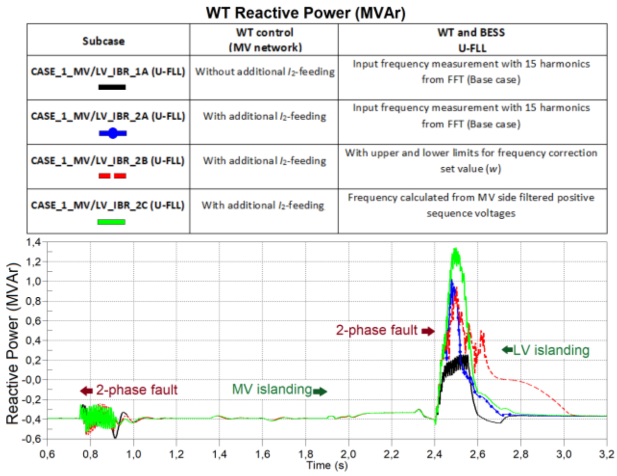

(b)

Figs. 15. Wind turbine, WT (a) active (P_{WT}) and (b) reactive power (Q_{WT}) at the WT connection point (Figs. 8, 10-12 and Tables II, III)

In islanded operation, I_2-current feeding of the WT during 2-phase short-circuit fault supports the U_1 voltage momentarily to a small extent (Fig. 13(b)), but worsens the voltage stability after the fault. Interestingly, the active (Fig. 15(a)) and reactive power (Fig. 15(b)) behavior of the WT is very different with the same control scheme during 2-phase short-circuit fault in grid-connected and islanded operation. Additional I_2-current feeding of the WT increases fluctuations in the active (Fig. 15(a)) and reactive powers (Fig. 15(b)) in islanded operation when compared to case (CASE_1_MV/LV_IBR_1A (U-FLL)) without additional I_2-current feeding. As a conclusion from these simulation results (Figs. 13-15) can be stated that the additional I_2-feeding of WT did not support the frequency and/or voltage stability and did not reduce the negative sequence voltage (U_2) during and after unbalanced 2-phase short-circuit faults. However, it must be noted that the 2-phase faults took place at different locations (Fig. 8) during grid-connected and islanded operation i.e. the location of the fault (distance from the HV/MV substation) also has affects on the behavior of voltages during faults in grid-connected operation.

It has been previously also stated in [3] and [6] that during LV microgrid islanded operation, the additional reactive current (I_Q) feeding is not recommended due to stability reasons and it did not support the voltage of the islanded LV microgrid. Therefore, especially during MV and LV islanded operation it is recommended to find new universal protection methods and principles which are not dependent on IBRs' I_2-current feeding although modification of U-FLL input (*CASE_1_MV/LV_IBR_2C (U-FLL)*) during islanded operation could reduce the frequency and voltage stability worsening to some extent when additional I_2-current feeding of the DER unit is utilized.

IV.1.2. Effect of Different U-FLL Inputs During Balanced Fault

Next the results with 100 % IBR-based generation in *CASE_1_MV_IBR* and *CASE_1_LV_IBR* (Fig. 8 and Table II) subcases (Table IV) during balanced 3-phase short-circuit are shown in Figs. 17-21. The control scheme differences of WT and BESS in the studied subcases are presented in Table IV and Figs. 16.

The aim of these simulation studies in this subsection (Table IV) was to examine the effect of U-FLL input differences on the transient stability of the DER unit during balanced 3-phase faults. In the study cases E and F (Table IV), the WT active power reduction at t=2.3 s (during MV islanded operation) was much smaller than in cases A-D (Table IV) and this can be also seen in the simulation results (Figs. 18-21) e.g. as a change in the voltages.

During 3-phase short-circuit fault, all the phase voltages will dramatically reduce and it is challenging for the frequency measurement functionality which is also used as an input for the U-FLL of WT and BESS. On the other hand, generally the fault current fed by DER unit (also IBR-based) increases or is at least maintained at the same level as before 3-phase fault.

Therefore, one of the studied options to modify U-FLL frequency input in this Section study cases CASE_1_MV/LV_IBR_3ph_E (U-FLL) and CASE_1_MV/LV_IBR_3ph_F (U-FLL) (Table IV) was current-based frequency measurement utilization during 3-phase faults (Fig. 16(b)).

Based on the simulation results (Figs. 18-21) of this subsection, cases E and F (Table IV) with current-based U-FLL seem to be the most promising from both frequency (Fig. 17) and voltage stability (Fig. 18) viewpoint during and after 3-phase faults.

Larger frequency deviation during 3-phase faults in cases A and D (Fig. 17) also has an effect on positive sequence voltage U_1 magnitude (Fig. 19(a)) and angle (Fig. 19(b)) in these cases which may also be challenging for the feeder protection. Also BESS positive sequence current I_1 behavior (Fig. 20) after 3-phase short-circuit fault clearance was less fluctuating in cases E and F (Table IV) with the current-based U-FLL (Fig. 16(b)).

TABLE IV
U-FLL DIFFERENCES IN SUBCASES OF CASE_1_MV/LV_IBR (FIGS. 8 AND 16, TABLE II) DURING BALANCED 3-PHASE FAULTS o)

Subcase *)	WT **) (MV network) U-FLL	BESS ***) (LV network) U-FLL
CASE_1_MV/LV_IBR_3ph_A (U-FLL)	Input frequency measurement with 15 harmonics from FFT (Base case), Figs. 2, 3	
CASE_1_MV/LV_IBR_3ph_B (U-FLL)	With sample and hold -logic, Fig. 16(a)	
CASE_1_MV/LV_IBR_3ph_C (U-FLL)	With upper and lower limits for frequency correction set value (w), Fig. 10	
CASE_1_MV/LV_IBR_3ph_D (U-FLL)	Input frequency measurement with 63 harmonics from FFT	
CASE_1_MV/LV_IBR_3ph_E (U-FLL) oo)	Current-based U-FLL, Fig. 16(b)	
CASE_1_MV/LV_IBR_3ph_F (U-FLL) oo)	Current-based U-FLL, Fig. 16(b)	Input frequency measurement with 15 harmonics from FFT (Base case), Figs. 2, 3

*)All subcases with U-FLL , **)Control without additional I_2-feeding, ***) Control with I_2-filtering, o) LV side phase voltages are utilized for WT and BESS frequency measurement with FFT if not otherwise stated, oo) At t=2.3 s (during MV islanded operation) WT active power reduction is much smaller than in other cases A-D

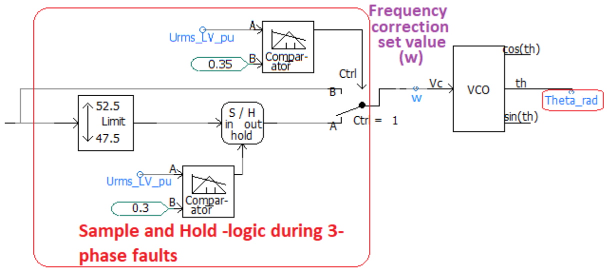

(a)

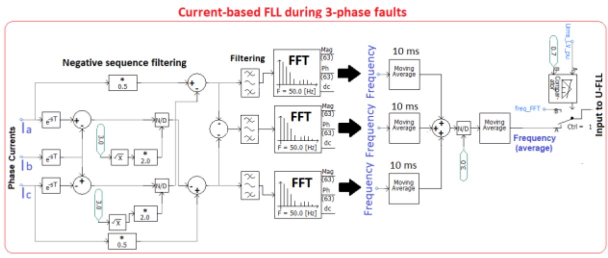

(b)

Figs. 16. (a) Sample and hold –logic and (b) current-based U-FLL of WT and BESS during 3-phase faults (Table IV)

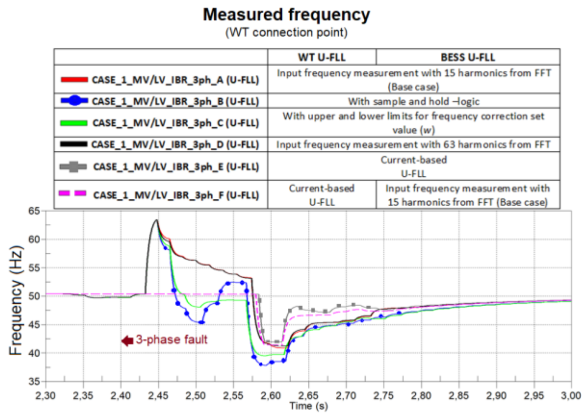

Fig. 17. Measured frequency at the WT connection point (Figs. 8, 11, 16 and Tables II, IV)

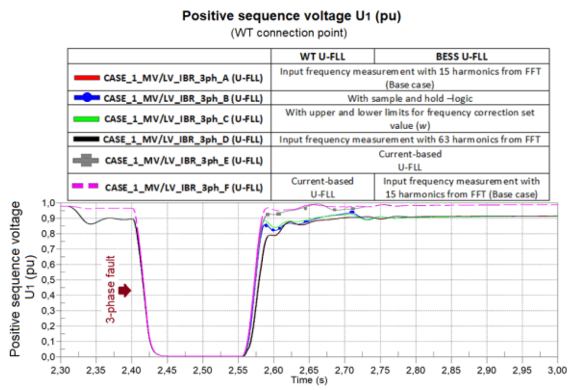

Fig. 18. Positive sequence voltage U_1 (pu) at the WT connection point (Figs. 8, 11, 16 and Tables II, IV)

However, also case B with the sample and hold -logic (Fig. 16(a), Table IV) and case C with the upper and lower limits (Fig. 10, Table IV) can provide improved frequency stability (Fig. 17) during and after 3-phase short-circuit faults in MV islanded operation.

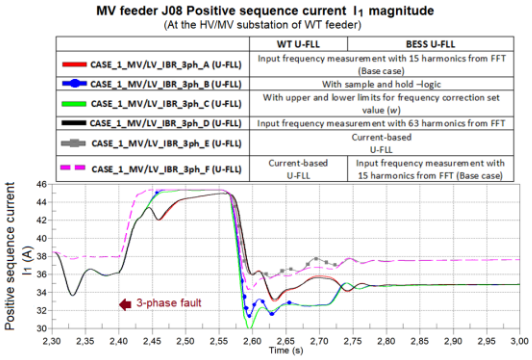

(a)

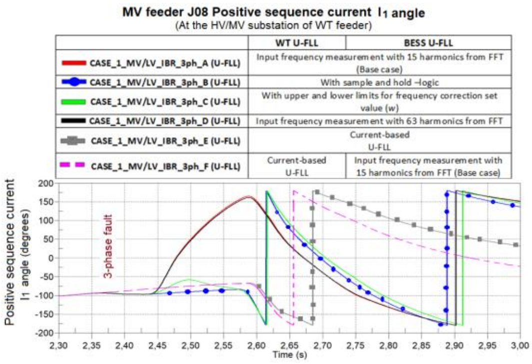

(b)

Figs. 19. MV feeder J08 (with WT) positive sequence current I_1 (a) magnitude and (b) angle at the HV/MV substation (Figs. 8, 11, 16 and Tables II, IV)

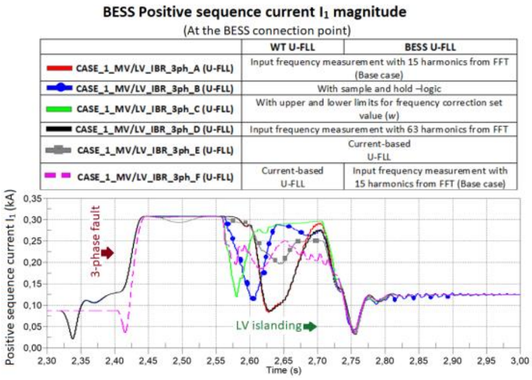

Fig. 20. Positive sequence current I_1 magnitude at the BESS connection point (Figs. 8, 11, 16 and Tables II, IV)

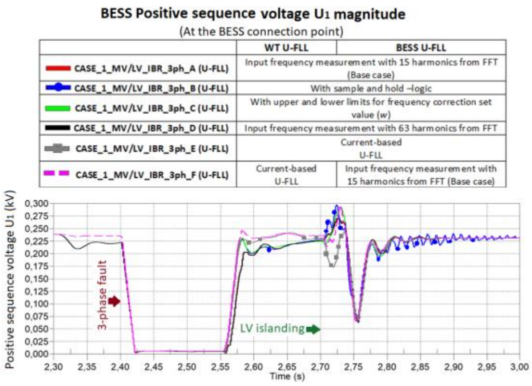

Fig. 21. Positive sequence voltage U_1 magnitude at the BESS connection point (Figs. 8, 11, 16 and Tables II, IV)

IV.2. Hybrid MV Microgrid

In Section IV.2 subcases, the total simulation time was t=30.0 s, transition to MV islanded (microgrid) operation with WT (Fig. 2) and SG (Fig. 5) happened at t=13.6 s.

In all simulations balanced 100 ms (at MV feeder J07 before Circuit-Breaker (CB) KP 639 opening, Fig. 5) 3-phase short-circuit happened between t=19.8-19.9 s.

IV.2.1. Effect of Different U-FLL Inputs During Balanced Fault

In this subsection, the simulation results from MV hybrid network with IBR (WT, Fig. 2) and SG (CASE_1_MV_HYBRID) (Fig. 5 and Table II) subcases (Table V) during balanced 3-phase short-circuit are shown in Figs. 23 and 24. The control scheme differences of WT U-FLL in subcases are presented in Table V and Figs. 22. The target of these simulation studies in this Section (Table V) was to study the effect of U-FLL input on the transient stability of the DER unit during balanced 3-phase faults like in previous subsection. However, in this subsection the studied MV hybrid microgrid also included SG (Fig. 5). Based on the simulation results of this subsection (Figs. 23 and 24), case B with the sample and hold -logic (Fig. 10, Table V) and case G with the frequency input from SG's rotating speed (Fig. 22(c), Table V) are the most promising solutions from both frequency (Fig. 23) and voltage stability (Fig. 24) viewpoint. However, the rotor speed of SG should be available for other IBR-based DERs in the MV microgrid with minimum communication time delay (see next subsection). In addition, it can be seen from simulation results (Fig. 23) that even if frequency stability seems to be good in case F with the frequency input from PSCAD frequency measurement component (Fig. 22(b), Table V), voltage stability is lost (Fig. 24). In the previous subsection, it was concluded that with 100 % IBR-based generation in MV microgrid utilization of current-based U-FLL during 3-phase fault was the most promising option.

TABLE V
U-FLL DIFFERENCES IN SUBCASES OF CASE_1_MV_HYBRID (FIGS. 5 AND 22, TABLE II) DURING BALANCED 3-PHASE FAULTS

Subcase $^{*)}$	WT $^{**),***)}$ U-FLL Differences
CASE_1_MV_HYBRID_3ph_A (U-FLL)	Input frequency measurement with 15 harmonics from FFT (Base case), Fig. 2
CASE_1_MV_HYBRID_3ph_B (U-FLL)	With sample and hold –logic, Fig. 16a
CASE_1_MV_HYBRID_3ph_C (U-FLL)	With upper and lower limits for frequency correction set value (w), Fig. 10
CASE_1_MV_HYBRID_3ph_D (U-FLL)	With rate limiter (5/s), Fig. 22(a)
CASE_1_MV_HYBRID_3ph_E (U-FLL)	Current-based U-FLL, Fig. 16b
CASE_1_MV_HYBRID_3ph_F (U-FLL)	Frequency input from PSCAD freq. measurement component, Fig. 22(b)
CASE_1_MV_HYBRID_3ph_G (U-FLL)	Frequency input from SG's rotating speed, Fig. 22(c)

$^{*)}$All subcases with U-FLL , $^{**)}$Control without additional I_2-feeding, $^{***)}$ LV side phase voltages are utilized for WT frequency measurement with FFT if not otherwise stated

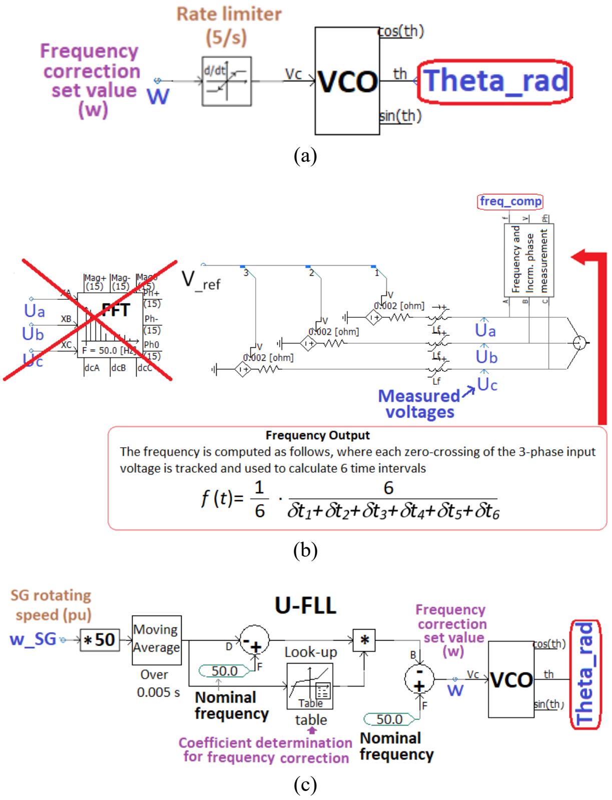

Figs. 22. (a) Rate limiter (5/s), (b) frequency input from PSCAD freq. measurement component and (c) frequency input from SG's rotating speed with U-FLL of WT and BESS during 3-phase faults (Table V)

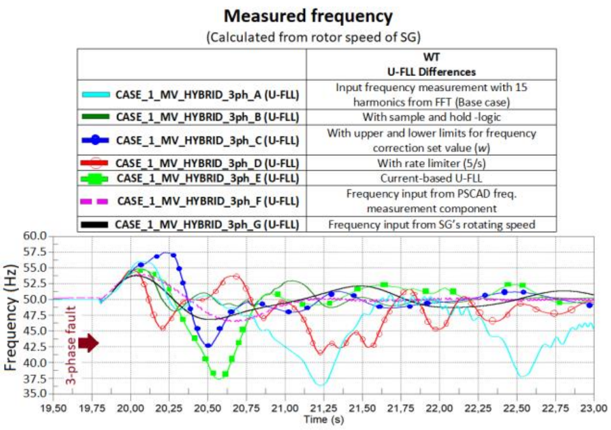

Fig. 23. Measured frequency at the SG connection point calculated from rotor speed of SG (Figs. 5, 22 and Table II, V)

Also in hybrid MV with SG case E with the current-based U-FLL (Table V) is stable during the 3-phase fault until transition from the current-based U-FLL back to the voltage-based U-FLL happens (Figs. 23 and 24). On the other hand, constant operation with current-based U-FLL (i.e. without transition from voltage-based U-FLL during 3-phase faults) is not feasible with weather-dependent generation because active power and current output goes to zero momentarily and fluctuates rapidly during normal operation according to weather variations.

Simultaneously, also the reactive power fluctuates depending on the used control method.

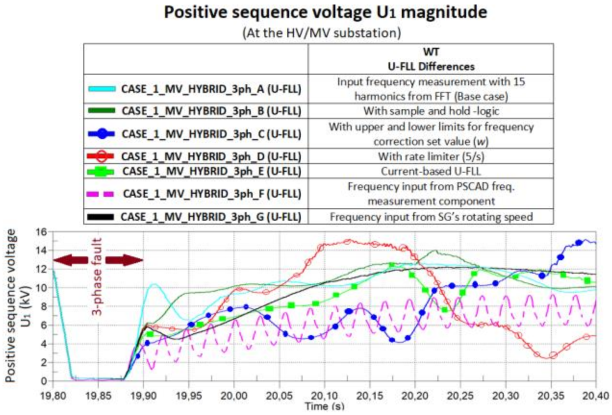

Fig. 24. Positive sequence voltage U_1 (kV) at the HV/MV substation (MV bus) (Figs. 5, 22 and Tables II, V)

Therefore, case B with the sample and hold -logic and case G with the frequency input from SG's rotating speed are more promising inputs for the DER units' U-FLL in the hybrid MV microgrids.

IV.2.2. Effect of U-FLL Input Related Communication Time Delay

Next the results from MV hybrid network with IBR (WT, Fig. 2) and SG (*CASE_1_MV_HYBRID*) (Fig. 5 and Table II) subcases (Table VI) during balanced 3-phase short-circuit are shown in Figs. 26 and 27. The focus is on the effect of communication time delay (15 or 40 ms) in *CASE_1_MV_HYBRID_3ph_G* where WT's U-FLL frequency input comes directly from the rotating speed of the SG. The idea of chosen 15 and 40 ms communication time delays is to show how important from transient stability point of view is to minimize the communication latency as well as signal processing related delays. Very low communication latencies could be achieved with high-speed wireless 5G/6G technologies or fiber optic solutions when measurement point of SG rotating speed is not too far away from the IBRs utilizing it as part of their U-FLL. On the other hand, communication time delay could be also possibly compensated to some extent, for example, in 5G networks by utilizing IEEE 1588 PTP-based time synchronization. In [38], 50 or 200 ms delayed frequency measurement of SG rotating speed, when it is used as input for *Pf*-control and U-FLL of BESS, was studied in order to see the effect of such communication delays on frequency stability and frequency support after the load change. However, in case of 3-phase faults such communication time delays are not applicable with U-FLL-based IBRs. It can be seen from the simulation results (Figs. 26 and 27) that, if U-FLL input from SG rotor speed is delayed 40 ms (Table VI), voltage stability (Fig. 27) is lost after short period of time. Therefore, the utilization of SG rotor speed as an input for IBRs with U-FLL can only be possible if reliable and very low-latency communication (e.g. 5G or 6G time-synchronized wireless communication) is available in the future MV and LV microgrids.

TABLE VI
U-FLL DIFFERENCES IN SUBCASES OF CASE_1_MV_HYBRID (FIGS. 5, 22 AND 25, TABLE II) DURING BALANCED 3-PHASE FAULTS

Subcase *)	WT **), ***) U-FLL Differences
CASE_1_MV_HYBRID_3ph_G (U-FLL)	Frequency input from SG rotating speed, Fig. 22c
CASE_1_MV_HYBRID_3ph_G_40 ms (U-FLL)	40 ms delayed frequency input from SG's rotating speed, Fig. 25
CASE_1_MV_HYBRID_3ph_G_15 ms (U-FLL)	15 ms delayed frequency input from SG's rotating speed, Fig. 25

*)All subcases with U-FLL , **)Control without additional I_2-feeding

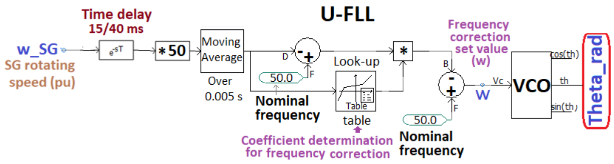

Fig. 25. 15/40 ms delayed frequency input from SG's rotating speed with U-FLL of WT and BESS during 3-phase faults (Table VI)

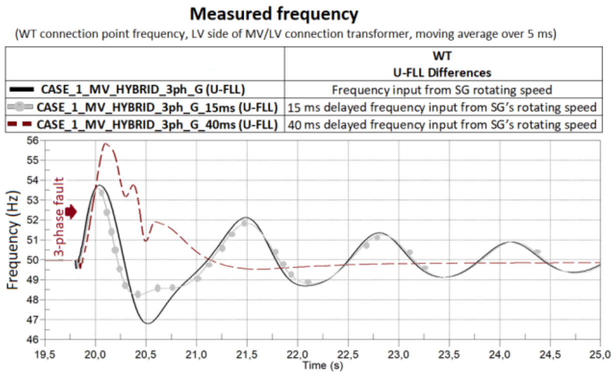

Fig. 26. Measured frequency at the WT connection point (Figs. 5, 22, 25 and Tables II, VI)

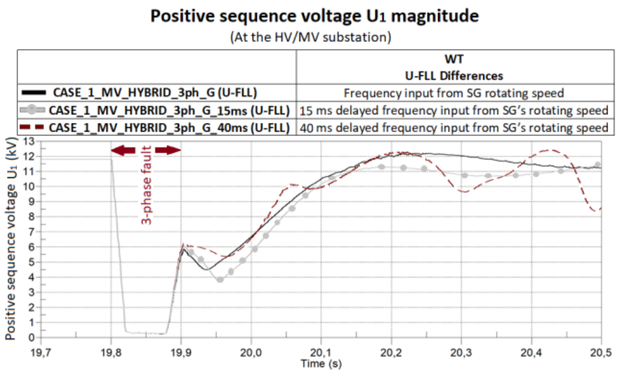

Fig. 27. Positive sequence voltage U_1 (kV) at the HV/MV substation (MV bus) (Figs. 5, 22, 25 and Tables II, VI)

IV.3. Small Hybrid HV Network

In this Section, the total simulation time was t=20.0 s with small hybrid HV network (CASE_2_HV_HYBRID, Fig. 7 and Table II) including BESSs (Fig. 4) and SG (Fig. 6).

In the simulations, 200 ms 2-phase unbalanced and 100 ms 3-phase balanced short-circuit happened at t=15.0 s in the middle of the 50 km HV line (Fig. 7).

IV.3.1. Effect of BESSs' Synchronization Method and Operation Mode During Unbalanced Fault

In this subsection, the simulation results from HV hybrid network with IBRs (BESSs, Fig. 4) and SG (Fig. 6) (CASE_2_HV_HYBRID) (Fig. 7 and Table II) subcases (Table VII) during 200 ms unbalanced 2-phase short-circuit (Fig. 7) are presented in Figs. 28 and 29.

The subcases with control scheme differences in BESS synchronization (PLL or U-FLL) and operation mode (discharging or charging) are presented in Table VII. The purpose of the simulation studies (Table VII) in this subsection was to examine the effect of BESS synchronization method (PLL or U-FLL) and operation mode on the frequency stability (Fig. 29) and total fault current (Figs. 28) during and after 2-phase short-circuit fault. It can be seen from the simulation results (Figs. 28 and 29) that, when BESSs' are synchronized with U-FLL instead of PLL (Table VII) first swing frequency stability after 2-phase short-circuit fault is slightly improved both during discharging and charging of the BESSs. Also one can see from Fig. 29 that, frequency stability is improved after 2-phase fault when the BESSs are in charging mode (i.e. acting as loads). In addition, Fig. 28(b) shows that during discharging of the BESSs 2-phase short-circuit current in phase A (rms, at the beginning of 50 km transmission line, Fig. 7) is slightly larger when the BESSs are synchronized by the U-FLL instead of PLL.

IV.3.2. Effect of BESSs' Synchronization Method and Operation Mode During Balanced Fault

In the following, the simulation results from HV hybrid network with IBRs (BESSs, Fig. 4) and SG (Fig. 6) (CASE_2_HV_HYBRID) (Fig. 7 and Table II) subcases (Table VII) during 100 ms balanced 3-phase short-circuit (Fig. 7) are presented in Fig. 30. The subcases with control scheme differences in BESS synchronization (PLL or U-FLL) and operation mode (discharging or charging) are presented in Table VIII.

The aim of the simulation studies (Table VIII) in this subsection was to study the effect of BESS synchronization method (PLL or U-FLL) and operation mode on frequency stability and total fault current (Fig. 30) during and after 3-phase short-circuit fault.

TABLE VII
BESS CONTROL SCHEME DIFFERENCES IN SUBCASES OF CASE_2_HV_HYBRID (FIG. 7, TABLE II) DURING UNBALANCED 2-PHASE FAULTS

Subcase	BESS **) Synchronization/Operation Mode
CASE_2_HV_HYBRID_2ph (Only SG, No BESSs) *)	-
CASE_2A_HV_HYBRID_2ph (PLL)	PLL / Discharging
CASE_2A_HV_HYBRID_2ph (U-FLL)	U-FLL / Discharging
CASE_2B_HV_HYBRID_2ph (PLL)	PLL / Charging
CASE_2B_HV_HYBRID_2ph (U-FLL)	U-FLL / Charging

*)Base case with SG and without IBRs (i.e. BESSs), **)Control without additional I_2-feeding

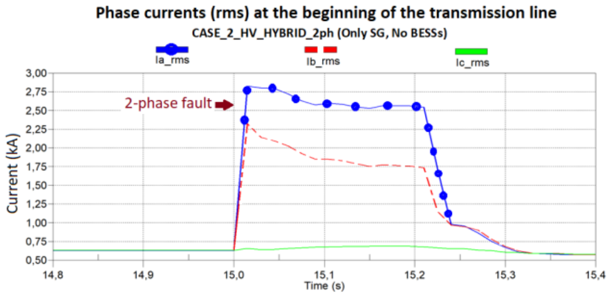

(a)

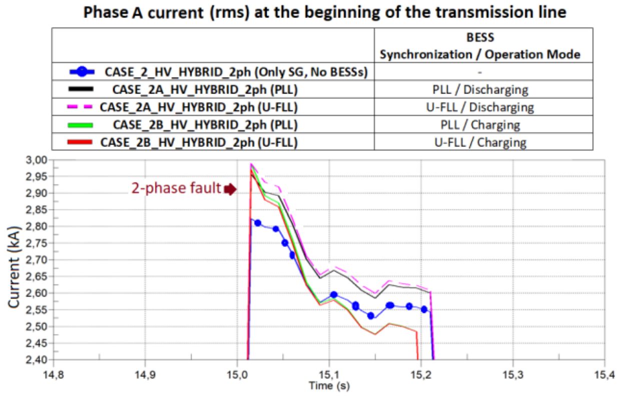

(b)

Figs. 28. (a) Phase currents (rms, kA) at the beginning of transmission line in CASE_2_HV_HYBRID_2ph (Only SG, No BESSs) and (b) phase current A (rms, kA) at the beginning of 50 km transmission line in different cases after 2-phase fault (Fig. 7 and Tables II, VII)

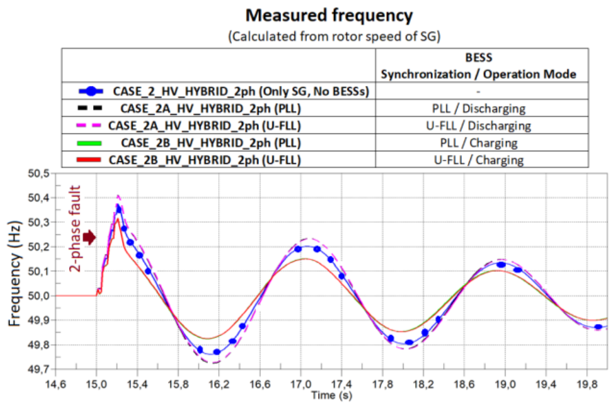

Fig. 29. Measured frequency at the SG connection point calculated from rotor speed of SG after 2-phase fault (Fig. 7 and Tables II, VII)

TABLE VIII
BESS CONTROL SCHEME DIFFERENCES IN SUBCASES OF CASE_2_HV_HYBRID (Fig. 7, Table II) DURING BALANCED 3-PHASE FAULTS

Subcase	BESS Synchronization / Op. Mode
CASE_2_HV_HYBRID_3ph (Only SG, No BESSs) *)	-
CASE_2A_HV_HYBRID_3ph (PLL)	PLL / Discharging
CASE_2A_HV_HYBRID_3ph (U-FLL)	U-FLL / Discharging
CASE_2B_HV_HYBRID_3ph (PLL)	PLL / Charging
CASE_2B_HV_HYBRID_3ph (U-FLL)	U-FLL / Charging

*)Base case with SG and without IBRs (i.e. BESSs)

It can be seen from the simulation results that differences in short-circuit currents (Fig. 30) between different cases during and after 3-phase faults (Table VIII) are much smaller than during and after 2-phase faults. In addition, measured frequencies in the different cases (Table VIII) during and after 3-phase faults were very similar without notable differences.

IV.4. Small Hybrid HV Network

In this Section IV.4, the total simulation time with small 100 % IBR-based HV network (*CASE_2_HV_IBR*, Fig. 9 and Table II) was t=20.0 s with BESSs (Fig. 4) as generating units. In the simulations, 200 ms 2-phase unbalanced and 100 ms 3-phase balanced short-circuit happened at t=15.0 s in the middle of the 50 km HV line (Fig. 9).

IV.4.1. Unbalanced Fault

In the following, the simulation results with 100 % IBR-based generation in *CASE_2_HV_IBR* (Fig. 9 and Table II and IX) during unbalanced 2-phase short-circuit are shown in Fig. 31. The BESS (Fig. 4) U-FLL details of the studied subcase are shown in Table IX/Fig. 10. It can be seen that in this case the frequency stability can be sufficiently maintained with BESSs utilizing upper and lower limits (Fig. 10, Table IX) in the U-FLL modification.

IV.4.2. Effect of Different U-FLL Modifications - Balanced Fault

In this subsection, the simulation results with 100 % IBR-based generation in *CASE_2_HV_IBR* (Fig. 9 and Table II and X) during balanced 3-phase short-circuit are shown in Figs. 32 and 33.

TABLE IX
BESS U-FLL IN CASE_2_HV_IBR (Fig. 9 AND Table II) DURING UNBALANCED 2-PHASE FAULTS

Subcase	BESS U-FLL
CASE_2_HV_IBR_2ph (U-FLL)	With upper and lower limits for frequency correction set value (w), Fig. 10

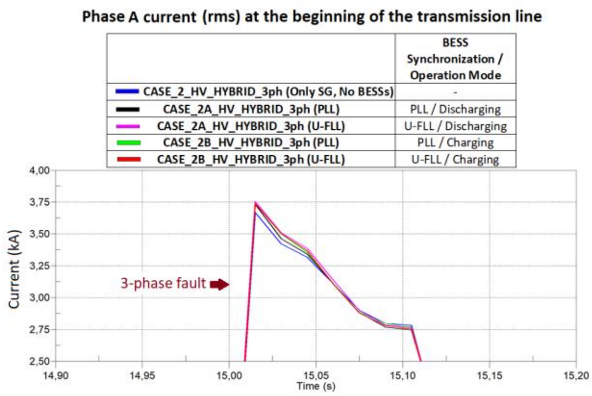

Fig. 30. Phase current A (rms, kA) at the beginning of 50 km transmission line in different cases after 3-phase fault (Fig. 7 and Tables II, VIII)

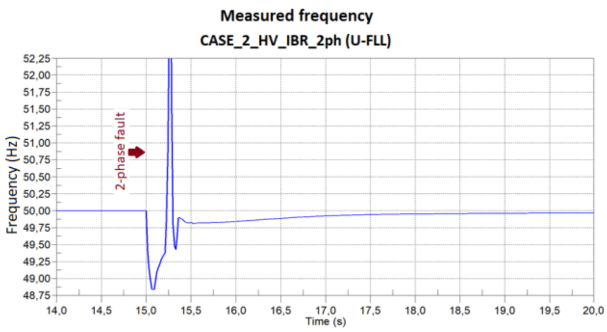

Fig. 31. Frequency measured at the connection point of BESS (CASE_2_HV_IBR_2ph (U-FLL)) (Fig. 9 and Tables II, IX)

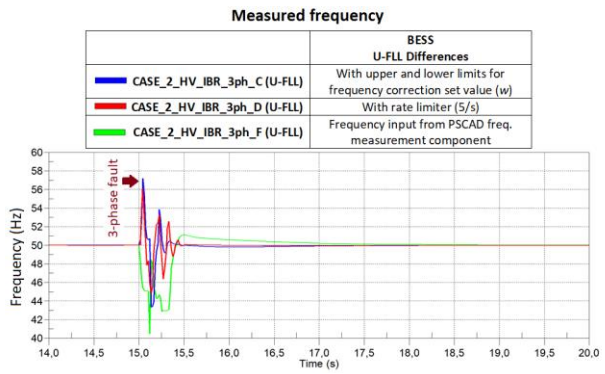

Fig. 32. Frequency measured at the connection point of BESS in different cases (Fig. 9 and Tables II, X)

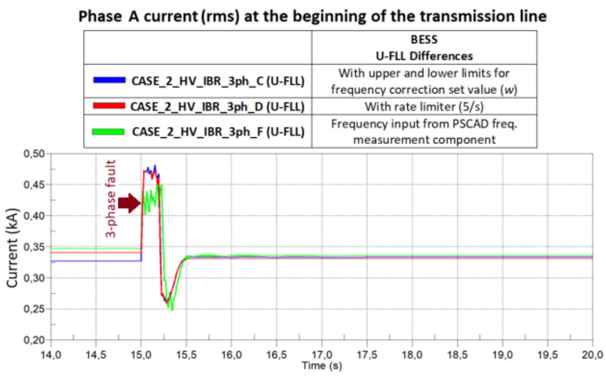

(a)

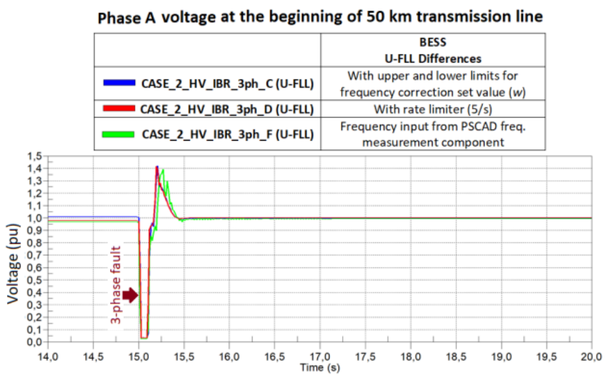

(b)

Figs. 33. (a) Phase A current (rms, kA) at the beginning of transmission line and (b) phase A voltage (pu) at the beginning of 50 km transmission line in different cases (Fig. 9 and Tables II, X)

TABLE X
BESS U-FLL DIFFERENCES IN SUBCASES OF CASE_2_HV_IBR (FIG. 9 AND TABLE II) DURING BALANCED 3-PHASE FAULTS

Subcase	BESS U-FLL Differences
CASE_2_HV_IBR_3ph_C (U-FLL)	With upper and lower limits for frequency correction set value (w), Fig. 10
CASE_2_HV_IBR_3ph_D (U-FLL)	With rate limiter (5/s), Fig. 22(a)
CASE_2_HV_IBR_3ph_F (U-FLL)	Frequency input from PSCAD freq. measurement component, Fig. 22(b)

TABLE XI
SUMMARY ABOUT THE UTILIZATION POTENTIAL OF DIFFERENT U-FLL MODIFICATIONS TO IMPROVE IBR FAULT BEHAVIOR & TRANSIENT FREQUENCY AND VOLTAGE STABILITY & FRT CAPABILITY IN DIFFERENT CASES (TABLE II) DURING UNBALANCED 2-PHASE AND BALANCED 3-PHASE SHORT-CIRCUIT FAULTS (EFFECT OF U-FLL MODIFICATION: - NEGATIVE, + POSITIVE, ++ VERY POSITIVE)

U-FLL Modification	CASE_1_MV_HYBRID 3-ph fault	CASE_1_MV_IBR 2-/3-ph fault	CASE_2_HV_IBR 2-/3-ph fault
Input frequency measurement with 15 harmonics from FFT	-	++$^{*)}$ and +$^{**)}$/-	
Input frequency measurement with 63 harmonics from FFT		/-	
With sample and hold –logic	++	/+	
With upper and lower limits for frequency correction set value (w)	+-	-$^{**)}$/+	+/+
Frequency calculated from MV side filtered positive sequence voltages		+$^{**)}$/	
With rate limiter (5/s)	-		/+
Current-based U-FLL	+-	/++	
Frequency input from PSCAD freq. measurement component	-		/+-
Frequency input from SG's rotating speed	++		

$^{*)}$ Without add. I_2-current feeding, $^{**)}$ With add. I_2-current feeding

The BESSs' (Fig. 4) U-FLL differences in the studied subcases are shown in Table X and Figures 11, 22(a) and 22(b). The target of these simulation studies in this subsection (Table X) was to examine the effect of U-FLL input on the frequency stability of the BESSs during balanced 3-phase short-circuit faults. The simulation results (Figs. 32 and 33) show that the frequency stability can be sufficiently maintained with BESSs utilizing the upper and lower limits in the case C (Fig. 10, Table X) as well as with rate limiter (5/s) (Fig. 22(a), Table X) in the case D for U-FLL modification.

V. Conclusion

In the future power systems with large-amount of GFM IBRs, it is important that their stability during faults can be ensured and transient frequency and voltage stability of the low-inertia power systems can be maintained during both grid-connected and islanded operation. In addition, the fault behavior and response of

GFM IBRs must be compatible with the distribution and transmission network protection principles both in the grid-connected and islanded operation. In this paper, the grid-forming and supporting U-FLL -based grid synchronization method for IBRs was used when the effect of different U-FLL modifications on the transient stability, FRT capability and fault behavior of IBRs were studied. Multiple PSCAD simulations were done with a main focus on islanded operation. The key study cases were presented in Table II and based on the results of the PSCAD simulations following conclusions were drawn from each key study case:

- *CASE_1_MV_IBR*: Additional I_2-current feeding of WT did not support the frequency and/or voltage stability and did not reduce the negative sequence voltage U_2 during and after unbalanced 2-phase short-circuit faults (location of the 2-phase fault during grid-connected operation partly affected). Therefore, especially during MV and LV islanded operation, it is recommended to develop new universal protection schemes which are not dependent e.g. on IBRs' I_2 - current feeding;
- *CASE_1_MV_HYBRID*: If U-FLL input from SG rotor speed is delayed 40 ms, voltage stability can be lost. Therefore, utilization of SG rotor speed as a frequency input for IBRs with U-FLL can be only possible if reliable and very low-latency communication (e.g. 5G or 6G wireless communication) is available in the future MV and LV microgrids;
- *CASE_2_HV_HYBRID*: When BESSs' were synchronized with the U-FLL instead of PLL, the first swing frequency stability after 2-phase short-circuit fault was slightly improved both during discharging and charging of the BESSs. In addition, the frequency stability was improved after 2-phase fault when the BESSs were in charging mode (i.e. acting as loads);
- *CASE_1_MV_IBR, CASE_1_MV_HYBRID* and *CASE_2_HV_IBR*: Table XI presents a summary about the utilization potential of different examined U-FLL modifications in order to ensure and improve the transient frequency and voltage stability as well as FRT capability in different cases during unbalanced 2-phase and balanced 3-phase short-circuit faults.

The future protection and management functionalities realization for microgrids and active distribution networks will require new control architecture development with increased focus on utilization of massive amount of measurement data from multiple sources with artificial intelligence and machine learning techniques, intelligent utilization of edge and cloud computing as well as increased virtualization of primary and secondary substation functionalities. Regarding to the needed future functionalities development, focus of the future studies needs to be, for instance, on the development of new universal and transient stability supporting protection methods and principles for grid-connected and islanded operation as well as on the examination of the utilization possibility of SG rotor speed in MV and LV microgrids as a frequency input for IBRs with U-FLL by wireless very reliable, low-latency time-synchronized communication methods.

References

[1] A. Tuohy, P. Dattaray, E. Farantatos, A. Kelly and E. Lannoye, *Implications of Reduced Inertia Levels on the Electricity System: Technical Report on the Challenges and Solutions for System Operations with Very High Penetrations of Non-Synchronous Resources* (EPRI, Palo Alto, CA, 2019).

[2] A.A. Memon, H. Laaksonen, K. Kauhaniemi, Microgrid Protection with Conventional and Adaptive Protection Schemes, In A. Anvari-Moghaddam, H. Abdi, B. Mohammadi-Ivatloo, N. Hatziargyriou (Ed.) *Microgrids*: *Advances in Operation, Control, and Protection*. (Springer, Cham., 2021).

[3] Laaksonen, H., Kauhaniemi, K., Voima, S., DG unit fault behavior and protection of LV microgrid, (2010) *International Review on Modelling and Simulations (IREMOS)*, 3 (3), pp. 353-367.

[4] H. Laaksonen, Grid Code Compatible Protection Scheme for Smart Grids, *The 23rd International Conference on Electricity Distribution ~CIRED 2015~*, 15-18 June, 2015, Lyon, France.

[5] H. Laaksonen, Protection of Future Active Distribution Networks with Distributed Generation, *~SEAPAC 2015~*, CIGRE Australia APB5, 17-18 March, 2015, Sydney, Australia.

[6] H. Laaksonen, *Technical Solutions for Low-Voltage Microgrid Concept*, Ph.D. dissertation. Dept. of Electrical and Energy Engineering, University of Vaasa, 2011.

[7] X. Wang, H. Wu, X. Wang, Impact of Reactive Current Injection Modes on Transient Stability of Grid-Following VSCs During Fault Ride-Through, *IEEE 13th International Symposium on Power Electronics for Distributed Generation Systems ~PEDG~*, 26-29 June, 2022, Kiel, Germany.

[8] R. Teodorescu, M. Liserre, P. Rodriguez, *Grid Converters For Photovoltaic And Wind Power Systems*, (Hoboken, NJ, USA: Wiley-IEEE Press, 2011).

[9] A. Luna et al., Grid voltage synchronization for distributed generation systems under grid fault conditions, *IEEE Trans. Ind. Appl.*, vol. 51, n. 4, 2015, pp. 3414-3425.

[10] X. Wang, F. Blaabjerg, Harmonic stability in power electronic-based power systems: concept modeling and analysis, *IEEE Trans. Smart Grid*, vol. 10, n. 3, 2019, pp. 2858-2870.

[11] M. G. Taul, X. Wang, P. Davari, F. Blaabjerg, An overview of assessment methods for synchronization stability of grid-connected converters under severe symmetrical grid faults, *IEEE Trans. Power Electron.*, vol. 34, n. 10, 2019, pp. 9655-9670.

[12] X. Wang, M. G. Taul, H. Wu, Y. Liao, F. Blaabjerg, L. Harnefors, Grid-Synchronization Stability of Converter-Based Resources - An Overview, *IEEE Open Journal of Industry Applications*, vol. 1, 2020, pp. 115-134.

[13] L. Zhang, L. Harnefors, H. Nee, Power-synchronization control of grid-connected voltage-source converters, *IEEE Trans. Power Syst.*, vol. 25, n. 2, 2010, pp. 809-820.

[14] R. Rosso, X. Wang, M. Liserre, X. Lu, S. Engelken, Grid-Forming Converters: Control Approaches, Grid-Synchronization, and Future Trends—A Review, *IEEE Open Journal of Industry Applications*, vol. 2, 2021, pp. 93-109.

[15] T. Dragičević, S. Vazquez, P. Wheeler, Advanced Control Methods for Power Converters in DG Systems and Microgrids, *IEEE Transactions on Industrial Electronics*, vol. 68, n. 7, 2021, pp. 5847-5862.

[16] S. Golestan, J. M. Guerrero, J. C. Vasquez, Three-phase PLLs: A review of recent advances, *IEEE Trans. Power Electron.*, vol. 32, n. 3, 2017, pp. 1894-1907.

[17] W. Zhang, J. Rocabert, J. I. Candela, P. Rodriguez, Synchronous power control of grid-connected power converters under asymmetrical grid fault, *Energies*, vol. 10, n. 7, 2017, pp. 1-21.

[18] Q.-C. Zhong, P.-L. Nguyen, Z. Ma, W. Sheng, Self-synchronized synchronverters: Inverters without a dedicated synchronization unit, *IEEE Trans. Power Electron.*, vol. 29, n. 2, 2014, pp. 617-

630.
[19] P. Rodriguez, A. Luna, M. Ciobotaru, R. Teodorescu, F. Blaabjerg, Advanced Grid Synchronization System for Power Converters under Unbalanced and Distorted Operating Conditions, *32nd Annual Conference on IEEE Industrial Electronics ~IECON 2006~*, 6-10 November, 2006, Paris, France.
[20] P. Rodríguez, A. Luna, I. Candela, R. Mujal, R. Teodorescu, F. Blaabjerg, Multiresonant Frequency-Locked Loop for Grid Synchronization of Power Converters Under Distorted Grid Conditions, *IEEE Transactions on Industrial Electronics*, vol. 58, n. 1, 2011, pp. 127-138.
[21] B. Fan, T. Liu, F. Zhao, H. Wu, X. Wang, A Review of Current-Limiting Control of Grid-Forming Inverters Under Symmetrical Disturbances, *IEEE Open Journal of Power Electronics*, vol. 3, 2022, pp. 955 – 969.
[22] T. Qoria, F. Gruson, F. Colas, G. Denis, T. Prevost, X. Guillaud, Critical clearing time determination and enhancement of grid-forming converters embedding virtual impedance as current limitation algorithm, *IEEE J. Emerg. Sel. Top. Power Electron.*, vol. 8, n. 2, 2020, pp. 1050-1061.
[23] X. Wang, M. G. Taul, H. Wu, Y. Liao, F. Blaabjerg, L. Harnefors, Grid-Synchronization Stability of Converter-Based Resources - An Overview, *IEEE Open Journal of Industry Applications*, vol. 1, 2020, pp. 115-134.
[24] D. Pan, X. Wang, F. Liu, R. Shi, Transient stability of voltage-source converters with grid-forming control: A design-oriented study, *IEEE J. Emerg. Sel. Top. Power Electron.*, vol. 8, n. 2, 2020, pp. 1019-1033.
[25] M. G. Taul, S. Golestan, X. Wang, P. Davari, F. Blaabjerg, Modeling of Converter Synchronization Stability Under Grid Faults: The General Case, *IEEE Journal of Emerging and Selected Topics in Power Electronics*, vol. 10, n. 3, 2022, pp. 2790-2804.
[26] I. Erlich, T. Neumann, F. Shewarega, P. Schegner, J. Meyer, Wind turbine negative sequence current control and its effect on power system protection, *IEEE Power & Energy Society General Meeting*, 21-25 July, 2013, Vancouver, BC, Canada.
[27] L. Yashen, J. H. Eto, B. B. Johnson, J. D. Flicker, R. H. Lasseter, H. N. Villegas Pico, G.-S. Seo, B. J. Pierre, A. Ellis, *Research Roadmap on Grid-Forming Inverters*, (Golden, CO: National Renewable Energy Laboratory, NREL/TP-5D00-73476, 2020).
[28] A. Hadjileonidas, Y. Li, T. C. Green, Comparative Analysis of Transient Stability of Grid-Forming and Grid-Following Inverters, *IEEE International Power Electronics and Application Conference and Exposition (PEAC)*, 04-07 November, 2022, Guangzhou,Guangdong, China.
[29] T. Liu, X. Wang, F. Liu, K. Xin, Y. Liu, Islanding Detection of Grid-Forming Inverters: Mechanism, methods, and challenges, *IEEE Electrification Magazine*, vol. 10, n. 1, 2022, pp. 30-38.
[30] S. Stanković, T. Van Cutsem, L. Söder, Fault-Current Injection Strategies of Inverter-Based Generation for Fast Voltage Recovery, *IEEE Transactions on Power Systems*, vol. 37, n. 2, 2022, pp. 1543-1553.
[31] R. Rosso, *Stability Analysis of Converter Control Strategies for Power Electronics-Dominated Power Systems*, Ph.D. dissertation, CAU Kiel, 2020.
[32] K. Strunz, K. Almunem, C. Wulkow, M. Kuschke, M. Valescudero, X. Guillaud, Enabling 100 % Renewable Power Systems Through Power Electronic Grid-Forming Converter and Control: System Integration for Security, Stability, and Application to Europe, *Proceedings of IEEE*, 2022, pp. 1-25.
[33] B. Shakerighadi, N. Johansson, R. Eriksson, P. Mitra, A. Bolzoni, A. Clark, H.-P. Nee, An overview of stability challenges for power-electronic-dominated power systems: The grid-forming approach, *IET Gener. Transm. Distrib*. vol. 23, 2022.
[34] A. Johnson, *Minimum specification required for provision of GB grid forming (GBGF) capability (formerly virtual synchronous machine/VSM capability)*, (National Grid ESO, Final Modification Rep. GC0137, Nov. 2021).
[35] National Grid ESO, *GC0137: Minimum Specification Required for Provision of GB Grid Forming (GBGF) Capability*, Final Modification Report GC0137, 2021.
[36] H. Shin, J. Jung, S. Oh, K. Hur, K. Iba, B. Lee, Evaluating the Influence of Momentary Cessation Mode in Inverter-Based Distributed Generators on Power System Transient Stability, *IEEE Transactions on Power Systems*, vol. 35, n. 2, 2020, pp. 1618-1626.
[37] H. Laaksonen, Universal Grid-forming Method for Future Power Systems, *IEEE Access*, vol. 10, 2022, pp. 133109-133125.
[38] H. Laaksonen, Improvement of Power System Frequency Stability With Universal Grid-Forming Battery Energy Storages, *IEEE Access*, vol. 11, 2023, pp. 10826-10841.
[39] H. Laaksonen, Islanding Detection with Universal Grid-forming Inverter-based Generation, *The 27th International Conference on Electricity Distribution ~CIRED 2023~*, 12-15 June, 2023, Rome, Italy.

Authors' information

University of Vaasa, School of Technology and Innovations, Electrical Engineering, Vaasa, Finland.

Hannu Laaksonen received his M.Sc. (Tech.) degree in 2004 in electrical power engineering from the Tampere University of Technology, Tampere, Finland, in 2004 and his Ph.D. (Tech.) degree in electrical engineering from the University of Vaasa, Vaasa, Finland, in 2011. His employment experience includes working as a research scientist at the VTT Technical Research Centre of Finland and at the University of Vaasa. He has previously worked as a principal engineer at ABB Ltd. in Vaasa. He is currently a professor of electrical engineering at the University of Vaasa. He is also Flexible Energy Resources –research team leader and manager of the Smart Energy Master's Program. His field of interests include the control and protection of low-inertia power systems and microgrids, active management of distributed and flexible energy resources in future smart energy systems as well as future-proof technology and market concepts for smart grids.